Analysis of the Global Horizontal Irradiation variability from WRF-Solar for the five cities of Brazil

Ana Cleide Bezerra Amorim[1], Samira de Azevedo Santos Emiliavaca[1], Alan Rodrigues de Sousa[1], Bruno do Nascimento e Silva[1], André Luiz de Oliveira Lira[1], João Vítor Fonseca de Mendonça[1], Gabriela Rocha Alves da Silva[1], Moisés Elias Nascimento Rufino da Costa[1]

[1] SENAI Innovation Institute for Renewable Energies, Natal (Brazil)

Abstract

Technological and economic advances in recent years have driven the expansion of solar energy in Brazil. However, challenges remain, particularly with regard to climate variability and the scarcity of reliable historical data. This study evaluates the performance of the WRF-Solar model in estimating global horizontal irradiance in five Brazilian regions that have different climates. Two sets of parameterizations (P1 and P2) were employed and compared with observational data obtained from solarimetric stations. Typical Meteorological Years were generated based on the National Solar Radiation Database. The hourly results showed a high correlation (> 0.8) between the simulations and the observations on more than 80% of days, particularly during dry periods. RMSE analysis reinforced the model's superior performance during the less rainy months. The differences between G1 and G2, as provided by the model, highlight the importance of sensitivity tests. In conclusion, WRF-Solar is a promising tool with the potential to enhance solar energy planning in the country.

Keywords: Solar energy, Numerical modeling, WRF, FARMS

1. Introduction

In recent years, the technological and economic obstacles that limited the expansion of solar energy in the Brazilian electricity matrix have been progressively overcome. However, challenges relating to energy supply variability and dependence on atmospheric conditions persist (Machado *et al*., 2016). Despite Brazil's high level of solar radiation (Pereira *et al*., 2017), accurately characterizing this resource is crucial due to its spatial and temporal variability. The scarce distribution of solarimetric stations makes it difficult to obtain long historical series of the relevant meteorological variables, which are fundamental for the generation of Typical Meteorological Years (TMY).

For solar projects, it is necessary to estimate TMYs in order to accurately represent a region's climatology and support the sizing of power generation systems. In this context, atmospheric modelling, such as the Weather Research and Forecasting (WRF) model, is a promising tool for estimating solar radiation variables in TMY months, particularly in areas with limited long-term observational data.

Numerical weather and climate prediction models such as WRF play a key role in meteorological centres and are widely used to predict atmospheric conditions and inform decisions in areas such as agriculture, water resources and transportation. More recently, they have also been used in the energy sector. There is a version of WRF adapted for solar energy studies called WRF-Solar. This specialised module accurately simulates the physical and chemical processes that occur in the atmosphere (Tinoco *et al.*, 2022; Mierzwiak *et al.*, 2022, 2023; Lee *et al.*, 2023; Amorim *et al*., 2024; Sawadogo *et al*., 2024), enabling detailed forecasts that support the solar industry.

Precipitation, temperature and wind speed are among the most frequently analysed meteorological variables. These variables are widely used by the scientific community to understand atmospheric behaviour (Comin *et al*., 2016; Onwukwe & Jackson, 2020; Srivastava *et al*., 2023). However, numerical forecasts have also become increasingly relevant to the energy sector, particularly with regard to solar irradiance and wind speed — variables that are directly related to the generation of renewable energy.

In the context of solar energy, obtaining accurate, high-resolution data on the spatial distribution of solar resources is crucial for optimising the planning and location of solar power plants and maximising their generation capacity.

10.18086/swc.2025.04.04 Available at http://proceedings.ises.org

Achieving this level of detail requires the use of numerical models, which provide information on the intensity and variation of solar radiation over time and space (Wind and Solar Atlas of Rio Grande do Norte, 2022; Solar Atlas of the State of Amapá, 2024). These models are fundamental to increasing operational efficiency in the energy sector and promoting the more effective management of natural resources.

Therefore, advancements in numerical modelling significantly impact climate forecasting and the planning and operation of sectors that depend on a detailed understanding of atmospheric phenomena to optimise operations and reduce risks. This study proposes evaluating the performance of the WRF-solar model in estimating global horizontal irradiance (GHI) in five different climatic regions of Brazil.

2. Materials and Methods

2.1 Study Area – Data Colletion

The study covers five different states, four of which are in Brazil's Northeast region and one of which is in the western part of São Paulo state (see figure 1).

Solarimetric stations were installed in the following five study areas: Sousa (PB) – ESA01, São João do Piauí (PI) – ESA02, Ilha Solteira (SP) – ESA03, Mossoró (RN) – ESA04 and Bom Jesus da Lapa (BA) – ESA05. Data was collected for each location throughout the year 2023. The solarimetric stations are equipped with temperature, relative humidity, wind speed, and global horizontal irradiance sensors. Data is collected every second and integrated at one-minute intervals by an acquisition system which can be accessed remotely via the internet.

Within the scope of the SENAI Institute for Innovation in Renewable Energy (ISI-ER), the control and quality assurance of solarimetric data follow a consolidated methodology based on a set of standardized tests, which include global, physical, comparative, and refinement tests (Da Silva *et al*., 2024). Global tests are applied to the entire time series and aim to identify discontinuities, recording failures, gaps, and errors in date and time. Physical tests evaluate the plausibility of the data based on physical limits, considering the presence of zero standard deviation and the consistency of the recorded parameters. Comparative tests verify consistency between parameters, while refinement tests analyze the temporal evolution of the data.

The Köppen climate classification (Alvares *et al*., 2013), illustrated in figure 1, categorizes the municipalities of Sousa (PB) and Bom Jesus da Lapa (BA) as belonging to the tropical climate with dry summer (As). Ilha Solteira (SP) – ESA03 has a tropical climate with dry winter (Aw), while Mossoró (RN) – ESA04 and São João do Piauí (PI) – ESA02 are classified as having a semi-arid climate (BSh).

The tropical climate (zone A) can occur with a dry winter ('w') or dry summer ('s'). The semi-arid BSh climate (B – dry; S – semi-arid; h – low latitude and altitude regions) is typical of Northeast Brazil (NEB) and represents 5.5% of the Brazilian territory (Alvares *et al*., 2013), predominating in areas with average annual rainfall below 800 mm and high temperatures throughout the year. Among the main characteristics of BSh are sparse and irregular rainfall, which can result in long periods of drought. These conditions are favorable for solar energy generation due to the high incidence of solar radiation in the region.

In the state of São Paulo, a subtropical climate (zone C) predominates approximately 66.9% of the territory, while about 33.2% is influenced by a tropical climate. Within this tropical portion, 30.8% have a tropical climate with a dry winter (Aw), the region where Ilha Solteira is located.

A subtropical climate is characterized by a wide annual temperature range, with hot summers and cold winters. Cold air masses are common during the winter, significantly reducing minimum temperatures, which are often below 18°C. These conditions favor solar energy generation, as the presence of these air masses generally inhibits cloud formation, resulting in clear skies and high levels of solar radiation. Rainfall in the state is evenly distributed throughout the year, with the highest volumes occurring during the austral spring and summer.

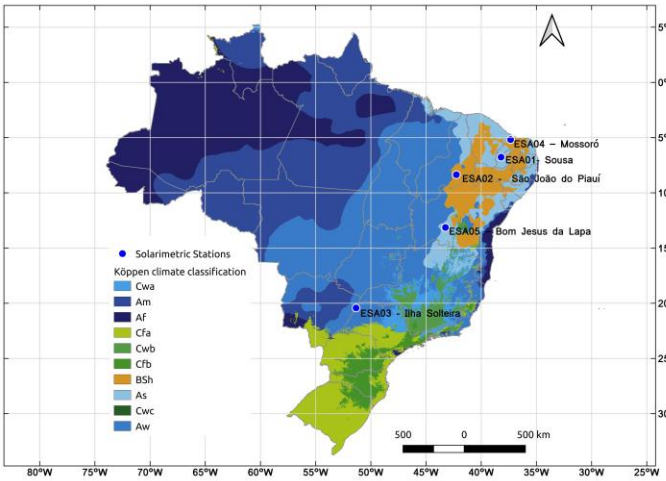

Figure 1: The Köppen climate classification map shows the locations of the solarimetric stations involved in this study: ESA01 – Sousa/PB, ESA02 – São João do Piauí/PI, ESA03 – Ilha Solteira/SP, ESA04 – Mossoró/RN and ESA05 – Bom Jesus da Lapa/BA. Source: Adapted from Álvarez *et al.*, 2013.

2.2 Mesoscale Atmospheric Modeling: WRF-Solar

The GHI for 12 typical months for five locations was simulated using the WRF model, version 4.3.3. A version of the WRF model has been developed for solar energy applications (WRF-Solar), incorporating improvements such as the inclusion of the irradiance components GHI, Gb (direct normal irradiance) and Gd (diffuse horizontal irradiance) (Jiménez et al., 2016). In addition to these improvements, the FARMS (Fast All-sky Radiation Model for Solar Applications) algorithm was implemented to calculate surface irradiance (Xie et al., 2016). This was also incorporated into the results as a second G estimate for analysis. Thus, two estimates of G were evaluated at each location: G1 (downward short wave flux at the ground surface, SWDOWN) and G2 (SWDOWN2: estimate from FARMS).

The main physical parameters are divided into five distinct categories: Microphysics, Clouds, the Planetary Boundary Layer, Land Cover Models and Long and Short Radiation (see Table 1). The selection of experiments (named P1 and P2) illustrated in Table 1 was previously carried out by Emiliavaca et al. (2024). The results showed that only ESA01 required two distinct experiments: P2 in the driest months and P1 in the rainy months. The other locations were represented by a single experiment throughout the year: P2 for ESA02 and P1 for ESA03, ESA04 and ESA05. This difference in the number of experiments reflects the particularities of the climate and the need for different models depending on the seasonal and regional conditions of each location.

Table 1: Physical parameters used in the experiments

Physical parameterizations	Code - Experiment	References
Microphysics (mp_physics)	Single Moment 5 class (4) - P1 e P2	Hong, Dudhia and Chen (2004)
Longwave radiation (ra_lw_physics)	RRTMG (4) - P1; RRTM (1) - P2	Iacono *et al*. (2008); Mlawer *et al*. (1997)
Shortwave radiation (ra_sw_physics)	RRTMG (4) - P1; Dudhia scheme (P2); FARMS (P1 e P2)	Iacono *et al*. (2008); Dudhia (1989)
Surface layer scheme (sf_sfclay_physics)	MYNN surface layer (5) - P1 e P2	Nakanishi and Niino (2009)
Land surface model (sf_surface_physics)	Noah Land Surface Mode (2) - P1 e P2	Niu *et al*. (2011)

Planetary boundary layer (bl_pbl_physics)	MYNN 2.5 level TKE (5) - P1 e P2	Nakanishi and Niino (2006)
Cumulus	Grell 3D (5) - P1; Kain-Fritsch scheme (1) - P2	Grell (1993), Grell and Devenyi (2002); Kain (2004)

To evaluate GHI, unique domains with a horizontal resolution of 6 km were created and centred on the latitude and longitude of each solarimetric station, as shown in figure 1. The input data for the simulations were obtained from ERA5, a reanalysis product from the European Centre for Medium-Range Weather Forecasts (ECMWF) (Hersbach and Dee, 2016). The outputs were generated every hour, with the first six hours discarded for adjustment (spin-up). Part of the simulation process was performed on the High Performance Processing Center (NPAD) Cluster at UFRN, in Natal, with the computing environment appropriately configured.

The 12 months that best represent the availability of solar resources are known as the Typical Meteorological Year (TMY) and are used to support the development of projects focused on harnessing this energy. The TMY months for each location were estimated using data from the National Solar Radiation Database (NSRDB) – National Renewable Energy Laboratory (NREL) (Sengupta et al., 2018), as shown in Table 2.

Table 2 also shows the rainiest and driest months for each location. In general, rainfall occurs between November and June, with variations between regions: ESA01 (November to May), ESA02, ESA03 and ESA05 (November to May), and ESA04 (January to June). Therefore, most rainfall occurs during the austral summer and autumn, while winter and spring tend to be drier.

Table 2: Estimated TMY months for each ESA with the respective wettest (blue tones) and driest (red tones) periods, indicating the wettest and driest months in which sensitivity tests were performed with experiments P1 and P2.

TMY	ESA01 - Sousa	ESA02 - São João do Piauí	ESA03 – Ilha Solteira	ESA04 - Mossoró	ESA05 – Bom Jesus da Lapa
JAN	2009 (P1)	2005 (P2)	2013 (P1) *	2008 (P1)	2011 (P1)
FEB	2015 (P1)	2003 (P2)	2007 (P1)	2017 (P1)	1999 (P1)
MAR	2001 (P1) *	2001 (P2) *	2003 (P1)	1999 (P1)	2000 (P1)
APR	2016 (P1)	2005 (P2)	2006 (P1)	2021 (P1) *	2003 (P1)
MAY	2013 (P1)	2013 (P2)	2010 (P1)	2021 (P1)	2017 (P1)
JUN	2007 (P2)	2004 (P2)	2017 (P1)	2013 (P1)	2017 (P1)
JUL	2004 (P2)	2000 (P2)	2010 (P1) **	2018 (P1)	2005 (P1) **
AUG	2002 (P2)	2000 (P2) **	2001 (P1)	2010 (P1)	2002 (P1)
SEP	2001 (P2)**	2020 (P2)	2001 (P1)	2018 (P1)	2003 (P1)
OCT	2017 (P2)	2013 (P2)	2016 (P1)	2013 (P1)	2013 (P1)
NOV	2005 (P2)	2017 (P2)	2006 (P1)	1998 (P1) **	2020 (P1)
DEC	2017 (P1)	2014 (P2)	2000 (P1)	2020 (P1)	2011 (P1) *

Rainiest month of the period (*); Month – Driest of the period (**)

2.3 Performance Metrics

The performance of the WRF-Solar model was analyzed using the following metrics: Pearson's correlation coefficient (r), root mean square error (RMSE), mean absolute error (MAE) and mean bias error (MBE). These metrics are commonly used in solarimetric data studies (Urraca *et al.*, 2018; Mierzwiak *et al.*, 2023; Thaker & Holler, 2023; Sawadogo *et al.*, 2024; Amorim *et al.*, 2024). The simulations are represented by S and the observed data by O:

$$r = \sum \frac{(S_i - \overline{S_i})(O_i - \overline{O_i})}{\sqrt{(S_i - \overline{S_i})^2 + (O_i - \overline{O_i})^2}} \qquad \text{eq (1)}$$

$$RMSE = \left[\frac{1}{N}\sum_{i=1}^{N}(S_i - O_i)^2\right]^{\frac{1}{2}} \quad \text{eq (2)}$$

$$nRMSE = \frac{RMSE}{\frac{1}{n}\sum_i^n O_i} x100 \quad \text{eq (3)}$$

$$MAE = \frac{1}{N}\sum_{(i=1)}^{N}|(S_i - O_i)| \quad \text{eq (4)}$$

$$nMAE = \frac{MAE}{\frac{1}{n}\sum_i^n O_i} x100 \quad \text{eq (5)}$$

$$MBE = \frac{1}{N}\sum_{i=1}^{N}(S_i - O_i) \quad \text{eq (6)}$$

$$nMBE = \frac{MBE}{\frac{1}{n}\sum_i^n O_i} x100 \quad \text{eq (7)}$$

These metrics were applied to hourly data, for which correlation results are presented daily, while other metrics are presented monthly.

3. Results and Discussion

The results of the performance of the WRF-Solar model in five Brazilian locations are presented and discussed. Figure 2 illustrates the daily correlations between observational data and model simulations on an hourly scale for two irradiances (G1 and G2), considering a significance level of 5%. Statistically significant and consistent correlations are observed throughout the year in all locations analysed, with values predominantly above 0.8 (black dashed lines), indicating temporal agreement between model estimates and observed measurements. Significant correlations ($p < 0.05$) were recorded on over 350 days per year, which reinforces the reliability of the WRF-Solar model for scientific and operational applications focused on modelling solar irradiance.

In seasonal terms, the highest correlations are observed during the driest months, when there is less cloud cover and greater atmospheric stability. This behaviour was notable between August and October in ESA01, from July to October in ESA02, from May to July in ESA03, between August and October in ESA04 and from April to October in ESA05. These patterns across different locations suggest that the model performs better under clear sky conditions, where direct irradiance is predominant and the impact of uncertainties in cloud representation is minimised. Various studies (Fountoukis *et al.*, 2018; Gueymard and Jiménez, 2018; Kim *et al.*, 2022; Thaker and Höller, 2023; Sawadogo *et al.*, 2024; Amorim *et al*., 2024) have discussed the ability of WRF-Solar in skies with few clouds and its limitations in areas with higher cloud concentrations around the world.

Conversely, the occasional decrease in correlations observed during certain periods may be associated with greater variability in cloud cover. This reflects a recognised limitation of the model when it comes to simulating more complex atmospheric conditions. Nevertheless, correlations greater than 0.8 on over 80% of days confirm WRF-Solar's ability to reproduce daily global irradiance variability in all analysed locations.

Figures 3 to 7 show the monthly analysis of the following statistical metrics: MBE, MAE, RMSE, NMBE, NMAE and NRMSE. These metrics are compared between the hourly estimates of WRF-Solar and the observed data for each location.

Analysis of these metrics revealed consistent differences in the performance of the two evaluated parameterisations (G1 – RRTMG/Dudhia; G2 – FARMS) across the five locations, reflecting distinct regional and seasonal climatic conditions.

Generally, both schemes performed better during the dry season (May to October), when clear sky conditions prevail. This is consistent with findings from other studies (Fountoukis *et al*., 2018; Gueymard & Jiménez, 2018; Kim *et al*., 2022; Amorim *et al*., 2024). During these months, the relative errors (nMAE and nRMSE) remained below 30%, indicating good agreement between the estimates and observations. Conversely, during the rainy season (November to April), there was a significant increase in errors and mean bias (nMBE), reflecting the models' difficulty in representing the high variability of cloudiness and atmospheric turbidity.

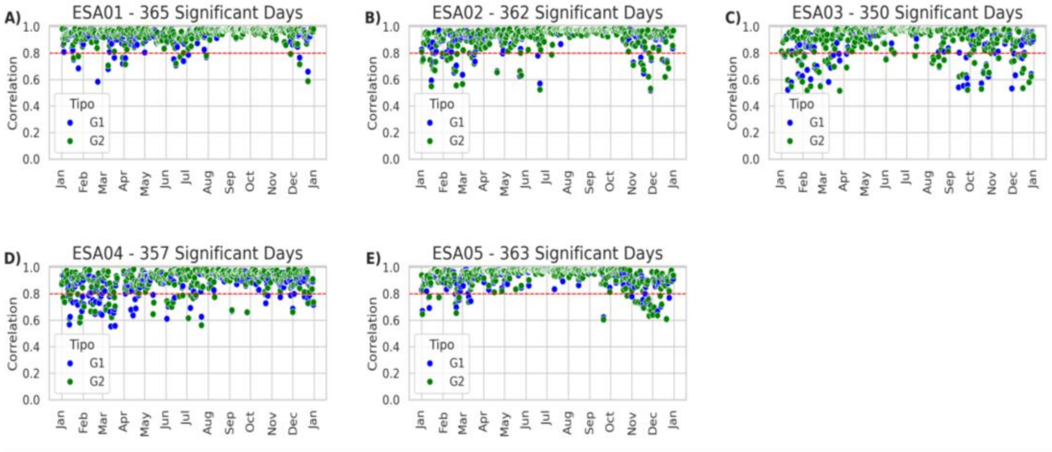

Figure 2: The daily correlation, with a statistical significance of 5%, between the WRF-Solar simulations and the observed data is shown for the five Brazilian regions. The black dashed line represents a correlation of 0.8.

Figure 3 (ESA01) shows that the mean bias (MBE and NMBE) indicates overestimation of the observed irradiance by both models (G1: RRTMG/Dudhia and G2: FARMS) throughout the year, with greater intensity in the G2 model simulated by FARMS, whose NMBE exceeded 30% in June. In contrast, G1 presented nNMBE values closer to zero, registering a slight underestimation in April (-0.22%), which indicates lower systematic bias and greater balance between seasons. These differences suggest that G1 is better suited to local atmospheric conditions.

The mean absolute error (MAE) and normalized mean absolute error (nMAE) values reinforce this trend, showing lower error magnitudes for the G1 configuration in most months. During the dry season, especially in August and October, the nMAE of G1 remained between 17% and 22%, reflecting good consistency in irradiance estimates. During the rainy months, however, a more pronounced increase in absolute error was observed, reaching values between 30% and 43%, due to more variable atmospheric conditions and greater cloud cover, which is typical of the wet season. G2 presented an MAE ranging from 89.4 to 96 W/m² and an nMAE ranging from 18.3 to 22.3% between August and October. Amorim *et al*. (2024) demonstrated an nMAE of 17% during the rainy season (the austral summer and autumn), 11% during the winter and 9% during the spring when using FARMS. This shows that there are locations where FARMS is efficient.

Analysis of the root mean square error (RMSE and nRMSE) confirms the expected seasonal behaviour. The highest values were observed in June: an RMSE of 202.9 W/m² (nRMSE 58.0%) for G1, and 222.5 W/m² (nRMSE 63.6%) for G2. This coincided with the transition period between the end of the rainy season and the start of the dry season, when there were still episodes of irregular cloudiness. The smallest errors occurred between August and October, with nRMSE values ranging from 23.2% to 27.5% for G1 and from 24.9% to 31.6%, which characterises the models' best performance under clear skies. Amorim *et al*. (2024) achieved nRMSE values ranging from 25% to 12% using G2 in Amapá, a region that poses significant challenges for solar energy modelling due to its high cloud cover throughout the year.

Sawadogo *et al*. (2024) found nRMSE values ranging from 9.6% to 15% when using WRF-Solar to forecast global horizontal irradiance at three stations in Ghana (Akwatia, Kumasi, and Kologo) in West Africa up to 72 hours in advance, and observed better performance under clear skies.

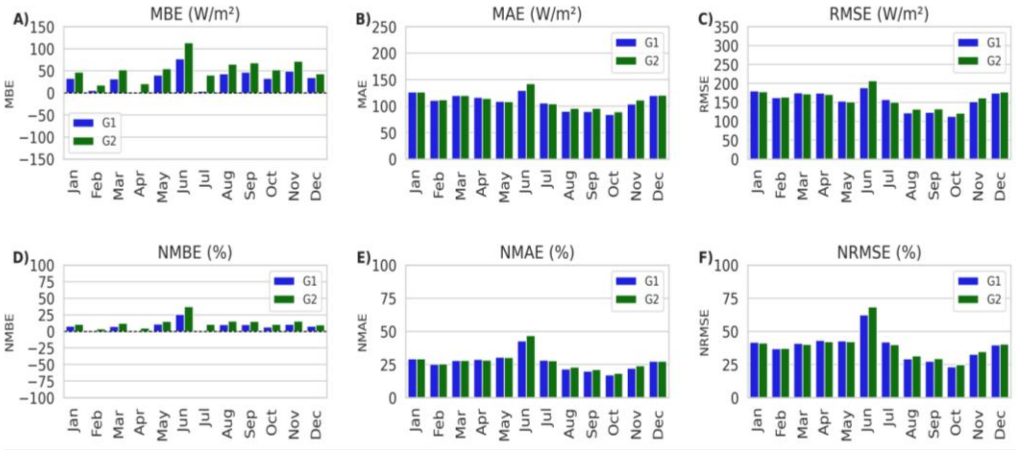

Figure 3. Root mean square error (RMSE), mean absolute error (MAE), and mean bias error (MBE) of the GHI (G1 and G2) for ESA01 - Sousa/PB based on hourly data between WRF-Solar simulations and observed data.

In São João do Piauí (ESA02), G1 is estimated as Dudhia only throughout the year. Similar results were obtained (see figure 4), with the mean error (MBE and nNMBE; see figures 4A and 4D) tending to overestimate irradiance in both parameterisations (Dudhia and FARMS), particularly in G2 (FARMS). Here, nNMBE values exceeded 20% in several rainy months. G1 showed more balanced performance, with lower biases and values close to zero during the dry season, reaching a maximum of 1.18% in July (see figure 4D). This indicates that the Dudhia estimate performs better in typical atmospheric conditions in the semi-arid region.

The pattern was similar for the mean absolute error (MAE and nNMAE, figures 4B and 4E) and the mean square error (RMSE and NRMSE, figures 4C and 4F), with lower errors recorded between July and September (NMAE <20% and NRMSE <27%, figures 4E and 4F), and worse performance between November and March, when the NRMSE exceeded 80%. The highest discrepancies were recorded in November, which coincided with the beginning of the rainy season and greater variability in cloud cover. Overall, G1 using Dudhia performed better in all metrics, with lower overestimation and smaller errors. In contrast, Amorim *et al*. (2024) obtained nRMSE values between 26% and 17% and nMAE values between 17% and 11% when using Dudhia in Amapá in the Amazon region.

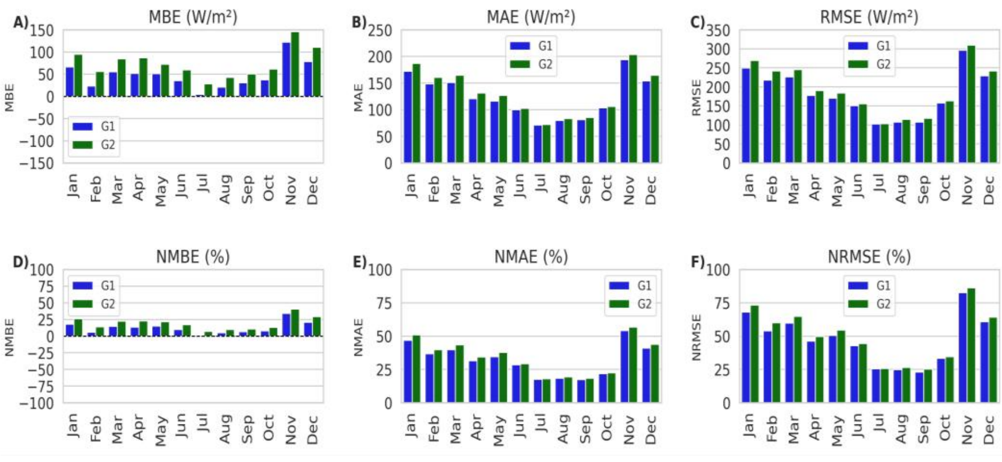

Figure 4. Root mean square error (RMSE), mean absolute error (MAE), and mean bias error (MBE) of the GHI (G1 and G2) for ESA02 – São João do Piauí/PI based on hourly data between WRF-Solar simulations and observed data.

At the Ilha Solteira station (ESA03) (figure 5), the influence of seasonality was also observed: the lowest nMBE occurred between May and July, with G1 (RRTMG) performing better and exhibiting reduced bias (between 1.5% and 4.9%; see figure 5D) and more balanced behaviour.

This trend is confirmed by the absolute error metrics (MAE and nMAE, figures 5B and 5E) and mean square error (RMSE and nRMSE, figures 4C and 4F). G1 exhibited lower mean and square errors in most months, with nRMSE values below 30% in July. However, in rainy months, errors exceeded 60%, again highlighting the limitations of models under variable atmospheric conditions.

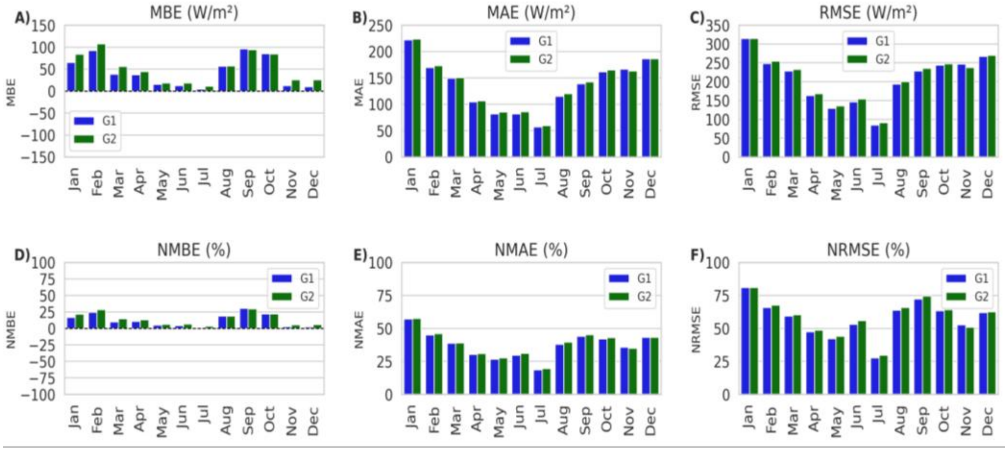

Figura 5. Root mean square error (RMSE), mean absolute error (MAE), and mean bias error (MBE) of the GHI (G1 andG2) for ESA03 – Ilha Solteira based on hourly data between WRF-Solar simulations and observed data.

In Mossoró (RN) (see figure 6), which is located in a semi-arid climate region (BSh), the performance of global horizontal irradiance estimates was favoured by the low atmospheric variability and high solar incidence that are typical of northeastern Brazil. The simulations showed good adjustment throughout the year, with better performance in the dry season (August to October), when the nRMSE was below 40% (see figure 6F). At the beginning of the year (January to March), errors increased (nRMSE >50%) due to increased cloud cover associated with the rainy season. The MBE indicated a tendency to overestimate in both parameterisations (figure 6A), which was more pronounced in G2; G1 showed less bias and better annual performance. The MAE and RMSE metrics confirm the robustness of the model under clear skies, with NMAE below 30% during the dry months. Overall, RRTMG and FARMS performed well in the semi-arid region, with G2 (FARMS) standing out by presenting lower MAE and RMSE. However, the MBE favoured G1 throughout the year.

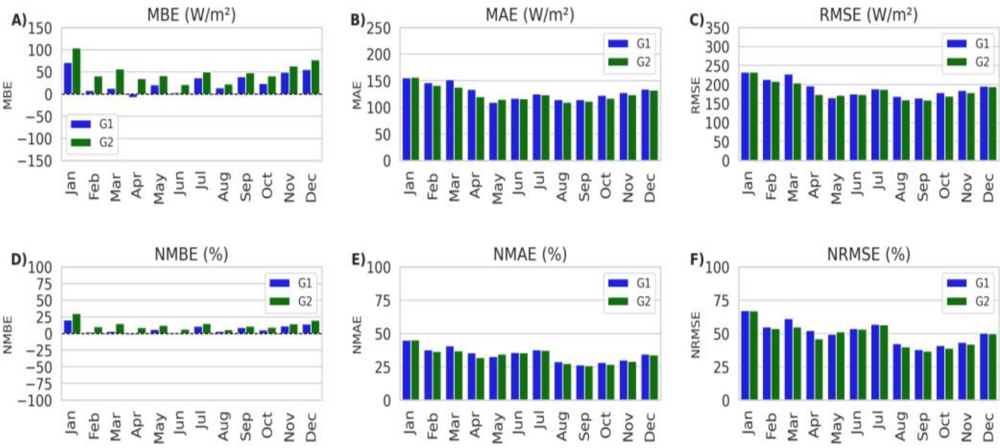

Figura 6. Root mean square error (RMSE), mean absolute error (MAE), and mean bias error (MBE) of the GHI (G1 and G2) for ESA04 - Mossoró/RN based on hourly data between WRF-Solar simulations and observed data.

Figure 7 shows the results for Bom Jesus da Lapa (ESA05). The two irradiance estimates performed excellently during the dry season, demonstrating high reliability under conditions of low cloud cover and atmospheric humidity (nRMSE < 25%; nMBE < 2%; nMAE < 20%). G1 maintained lower bias, while G2 showed better adjustment under clear skies from September onwards (see figure 7D). The RMSE was lower in G2 between January and August (Figure 7C), and the MAE also indicated slightly better performance of G2 between January and September (Figure 7B). However, the BEM (Figure 7A) revealed lower values for G2 only in July and September. This indicates that, although G2 shows good point accuracy in certain periods, it still tends to overestimate throughout the year.

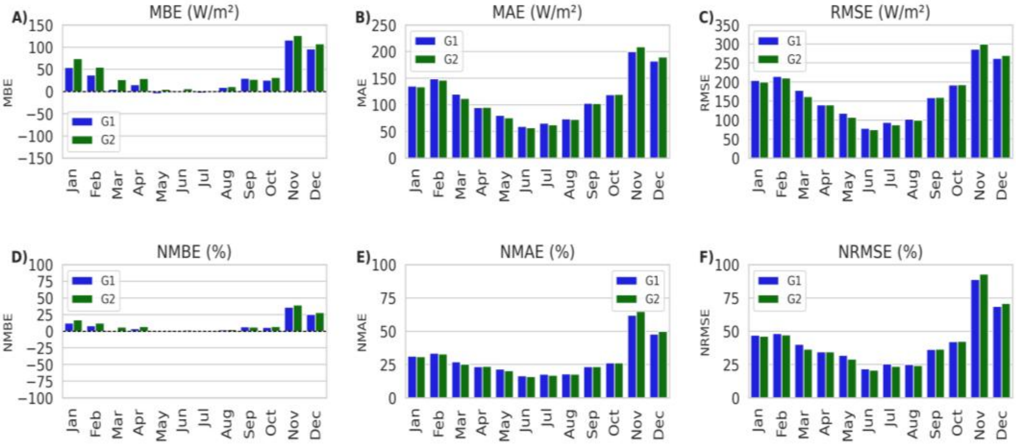

Figura 7: Root mean square error (RMSE), mean absolute error (MAE), and mean bias error (MBE) of the GHI (G1 and G2) for ESA05 - Bom Jesus da Lapa/BA based on hourly data between WRF-Solar simulations and observed data.

Generally, RMSE values below 100 W/m² were exclusively observed in Bom Jesus da Lapa/BA and Ilha Solteira/SP in June, July and August. The lowest RMSE value recorded was 75.02 W/m² in G2 in Bom Jesus da Lapa/BA in June, followed by 78.73 W/m² in G1. Values close to 100 W/m² were also observed in São João do Piauí/PI between July and September. All cities presented values in the range between 100 and 150 W/m², except Mossoró, which recorded RMSEs above this limit in all months. The lowest value was 158 W/m² in September by G2.

Conversely, the highest RMSEs (above 250 W/m²) were found in Bom Jesus da Lapa/BA and Ilha Solteira/SP, as well as in ESA02 – São João do Piauí/PI, from November to February. The highest value recorded in Mossoró was 232.86 W/m² in January by G1.

Overall, the results indicate that, when configured with RRTMG/Dudhia (G1) parameterisations, WRF-Solar performs better and shows greater seasonal stability in estimating global horizontal irradiance in the different regions evaluated here. These parameterisations can be applied in combination or in isolation and adapt well to local atmospheric characteristics, demonstrating consistency in the country's different climatic conditions.

Although the FARMS (G2) scheme is simple to implement and integrates directly with shortwave parameterisations, it was ineffective in correcting systematic errors in this study based on observational data from 2023. A tendency to overestimate was observed in several climatic contexts. It is worth noting that a typical meteorological year (TMY) was generated based on WRF-Solar simulations, and the estimates were evaluated over the course of a full annual cycle. This reinforces the representativeness and robustness of the obtained results.

Nevertheless, the FARMS scheme shows promise for use in complementary studies, particularly in sensitivity tests combining it with other shortwave radiation parameterisations under more complex atmospheric conditions.

Thus, the analysis shows that, although WRF-Solar has a good overall ability to reproduce irradiance variability in Brazil, local adjustments and additional calibrations are required to minimise the impact of atmospheric variability and enhance the reliability of simulations at various temporal and regional scales. This evidence strengthens the basis for the conclusions presented below, which summarise the overall performance of the radiation schemes evaluated and their implications for modelling solar irradiance in Brazil.

4. Conclusions

The study showed that WRF-Solar is effective in estimating global horizontal irradiance in different regions of Brazil, with daily correlations above 0.8 for most of the analyzed days. The best performance occurred during the least rainy period, from May to October, when clear skies and greater radiative stability prevail.

A joint assessment of the five locations revealed significant differences between the G1 and G2 estimates, which were associated with different climatic conditions and regional cloud cover. G1, which was estimated using the RRTMG and Dudhia schemes in combination or separately depending on the location, performed consistently better. It produced lower mean and quadratic errors (MAE and RMSE), lower bias (MBE) and a higher correlation with observations. These results suggest that traditional shortwave parameterizations of WRF (RRTMG/Dudhia) more accurately represent the radiative regime under different atmospheric conditions, particularly in tropical and semi-arid regions.

Conversely, while the FARMS (G2) parameterization performs well under clear skies, it was unable to correct the observed systematic errors and tended to overestimate irradiance in several scenarios. Nevertheless, FARMS is a promising tool as it can easily be integrated into different shortwave radiation schemes. This allows new sensitivity tests to be conducted and paves the way for future combinations that could potentially improve the model's radiative estimates.

The differences observed between G1 and G2 emphasize the importance of evaluating the interaction between radiation schemes and regional atmospheric variability, given that seasonality and cloud cover directly influence the accuracy of solar irradiance estimates.

In summary, G1 (RRTMG/Dudhia) was more suitable for local radiative modelling applications in the analyzed locations. Despite the good results obtained, atmospheric variability still poses challenges to the accuracy of estimates, reinforcing the need for specific adjustments to regional conditions.

To further this analysis, we intend to segment the results by clear, partly cloudy and cloudy days. This will enable us to assess the predictive capacity of WRF-Solar more accurately and indicate ways to improve the combined use of FARMS with other shortwave radiation parameterizations. This will expand the model's potential in different climatic contexts in Brazil.

5. Acknowledgments

This research was carried out as part of the activities of the National Institute for Technological Development of Photovoltaic Solar Energy Applications (INCT-DAESF), funded by the Brazilian agencies CNPq and MCTI under process number 408486/2024-4. The authors would like to thank the SENAI Institute for Innovation in Renewable Energy for its support and infrastructure; CTG Brasil, for its financial contribution to the ANEEL PD-10381-0620/2020 project; and TotalEnergies, for its current financial contributions to the ANP 23980-6 and ANP 24118-2 projects. The authors would like to thank ISI-ER for their support in the development of this work and TotalEnergies for the current financial support under the ANP PD-24118-2 project.

6. References

Kim, J.H., Jimenez, P.A., Sengupta, M., Yang, J., Dudhia, J., Alessandrini, S., Xie, Y., 2021. The WRF-Solar Ensemble Prediction System to Provide Solar Irradiance Probabilistic Forecasts. Journal of Photovoltaics 12, 1233–1235. https://doi.org/10.1109/JPHOTOV.2021.3134067

Amorim, A.C.B. *et al*. (2024). Analysis of WRF-solar in the estimation of global horizontal irradiation in Amapá, northern Brazil. Renewable Energy, 235, 124290. [https://doi.org/10.1016/j.renene.2024.124290].

C. A. Alvares, J. L. Stape, P. C. Sentelhas, J. L. M. Gonçalves, G. Sparovek, Köppen's climate classification map for Brazil, Meteorologische Zeitschrift. 22(6) (2013) 711-728. doi:10.1127/0941-2948/2013/0507

Emiliavaca, S.A.S., Amorim, A.C.B., Dantas, V.A., Sousa, A.R., Freire, J.L.M. (2024). Testes de sensibilidade utilizando o WRF-Solar na estimativa da irradiância global horizontal em cinco regiões climáticas do Brasil. Anais do Congresso Brasileiro de Energia Solar (CBENS 2024), Natal: ABENS. Disponível em: https://anaiscbens.emnuvens.com.br/cbens/article/view/2537/2506 (acesso em 28 abr. 2025).

Jimenez, P.A., Haupt, S.E., Ruiz-Arias, J.A. (2016). Short-term solar radiation forecasting with WRF-Solar: Impact of parameterization choice and aerosol prediction. Solar Energy, 146, 122–138.

Xie, Y., Sengupta, M., Dudhia, J. (2016). A fast all-sky radiation model for solar applications (FARMS): Model development and validation. Solar Energy, 135, 435–445.

Sengupta, M., *et al*. (2018). The national solar radiation data base (NSRDB). Renewable and Sustainable Energy Reviews, 89, 51–60.

Machado, I.S., Borba, B.S.M.C., Maciel, R.S. (2016). Modeling distributed PV market and its impacts on distribution system: A Brazilian case study. IEEE Latin America Transactions, 14(11), 4520–4526.

Pereira, E.B., *et al*. (2006). Atlas Brasileiro de Energia Solar. São José dos Campos: Instituto Nacional de Pesquisas Espaciais (INPE).

Comin, A.N., Souza, R.B., Acevedo, O.C., Anabor, V., 2016. Análise do desempenho do modelo Weather Research and Forecasting (WRF) com diferentes esquemas de microfísica e camada limite planetária na Ilha Deception, Antártica. Revista Brasileira de Meteorologia 31 (4), 415–427. https://doi.org/10.1590/0102-778631231420150027

Governo do Estado do Rio Grande do Norte, 2022. Atlas Eólico e Solar do Estado do Rio Grande do Norte. Instituto SENAI de Inovação – Energias Renováveis (ISI-ER), SEDEC, Coordenadoria de Desenvolvimento Energético, Natal.

Grell, G.A., 1993. Prognostic Evaluation of Assumptions Used by Cumulus Parameterizations. Mon. Wea. Rev. 121, 764–787. https://doi.org/10.1175/1520-0493(1993)121<0764:PEOAUB>2.0.CO;2

Grell, G.A., Devenyi, D., 2002. A generalized approach to parameterizing convection, combining ensemble and data assimilation techniques. Geophys. Res. Lett. 29 (14), 38–1–38–4. https://doi.org/10.1029/2002GL015311

Gueymard, C.A., Jimenez, P.A., 2018. Validation of real-time solar irradiance simulations over Kuwait using WRF-solar. In: the 12th International Conference on Solar Energy for Buildings and Industry, EuroSun2018, Rapperswil, Switzerland.

Hay, B., 2016. Drone tourism: a study of the current and potential use of drones in hospitality and tourism. CAUTHE 2016: The changing landscape of tourism and hospitality: the impact of emerging markets and emerging destinations, Sydney, 8–11 February.

Hersbach, H., Dee, D., 2016. ERA5 Reanalysis is in Production. ECMWF Newsletter, 147. https://www.ecmwf.int/en/newsletter/147/news/era5-reanalysis-production

Hong, S.-Y., Dudhia, J., Chen, S.-H., 2004. A revised approach to ice microphysical processes for the bulk parameterization of clouds and precipitation. Mon. Wea. Rev. 132, 103–120.

Iacono, M.J., Clough, S.A., Mlawer, E.J., Shephard, M.W., Collins, W.D., and Pincus, R., 2008. Radiative forcing by long-lived greenhouse gases: Calculations with the AER radiative transfer models. J. Geophys. Res.: Atmospheres 113 (D13).

J. Dudhia, 1989. Numerical study of convection observed during the winter monsoon experiment using a mesoscale two-dimensional model. J. Atmos. Sci. 46, 3077–3107.

Kim, J.H., Jimenez, P.A., Sengupta, M., Yang, J., Dudhia, J., Alessandrini, S., Xie, Y., 2021. The WRF-Solar Ensemble Prediction System to Provide Solar Irradiance Probabilistic Forecasts. Journal of Photovoltaics 12, 1233–1235. https://doi.org/10.1109/JPHOTOV.2021.3134067

Long, C.N., Shi, Y., 2008. An automated quality assessment and control algorithm for surface radiation measurements. The Open Atmospheric Science Journal 2 (1), 23–37. https://doi.org/10.2174/1874282300802010023

Mierzwiak, M., Kroszczyński, K., Araszkiewicz, A., 2023.WRF parameterizations of short-term solar radiation forecasts for cold fronts in Central and Eastern Europe. Energies 16(13), 5136.https://doi.org/10.3390/en16135136

Mlawer, E.J., Taubman, S.J., Brown, P.D., Iacono, M.J., Clough, S.A., 1997. Radiative transfer for inhomogeneous atmospheres: RRTM, a validated correlated–k model for the longwave. J. Geophys. Res. 102, 16663–16682. https://doi.org/10.1029/97JD00237

Nakanishi, M., Niino, H., 2009. Development of an improved turbulence closure model for the atmospheric boundary layer. J. Meteor. Soc. Japan 87, 895–912. https://doi.org/10.2151/jmsj.87.895

Niu, G.-Y., Yang, Z.-L., Mitchell, K.E., Chen, F., Ek, M.B., Barlage, M., Kumar, A., Manning, K., Niyogi, D., Rosero, E., Tewari, M., Xia, Y., 2011. The community Noah land surface model with multiparameterization options (Noah-MP): 1. Model description and evaluation with local-scale measurements. J. Geophys. Res. 116 (D12), D12109. https://doi.org/10.1029/2010JD015139

Onwukwe, C.H., Jackson, P.L., 2020. Meteorological downscaling with WRF model, version 4.0, and comparative evaluation of planetary boundary layer schemes over a complex coastal airshed. J. Atmos. Oceanic Technol. 37 (6), 1223–1244. https://doi.org/10.1175/JTECH-D-19-0212.1

Onwukwe, C.H., Jackson, P.L., 2020b. Meteorological downscaling with WRF model, version 4.0, and comparative evaluation of planetary boundary layer schemes over a complex coastal airshed. J. Appl. Meteor. Climatol. 59, 1295–1319. https://doi.org/10.1175/JAMC-D-19-0212.1

Pereira, E.B., Martins, F.R., Gonçalves, A.R., Costa, R.S., Lima, F.L., Rüther, R., Abreu, S.L., Tiepolo, G.M., Pereira, S.V., Souza, J.G., 2017. Atlas Brasileiro de Energia Solar, 2ª ed. São José dos Campos: INPE, 80 p. http://doi.org/10.34024/978851700089

Sawadogo, W., Fersch, B., Bliefernicht, J., Meilinger, S., Rummler, T., Salack, S., Guug, S., Kunstmann, H., 2024. Evaluation of the WRF-Solar model for 72-hour ahead forecasts of global horizontal irradiance in West Africa: A case study for Ghana. Solar Energy 263, 24–38. https://doi.org/10.1016/j.solener.2024.03.016

Srivastava, A.K., Ullrich, P.A., Rastogi, D., Vahmani, P., Jones, A., Grotjahn, R., 2023. Assessment of WRF (v 4.2.1) dynamically downscaled precipitation on subdaily and daily timescales over CONUS. Geosci. Model Dev. 16, 3699–3722. https://doi.org/10.5194/gmd-16-3699-2023

Thaker, J.A., Höller, R., 2023. Evaluation of High Resolution WRF Solar. Energies 16 (8), 3518. https://doi.org/10.3390/en16083518

Urraca, R., Huld, T., Gracia-Amillo, A., Martinez-de-Pison, F.J., Kaspar, F., Sanz-Garcia, A., 2018. Evaluation of global horizontal irradiance estimates from ERA5 and COSMO-REA6 reanalyses using ground and satellite-based data. Solar Energy 164, 339–354. https://doi.org/10.1016/j.solener.2018.02.059